RESEARCH ARTICLE

Key Points:
- Development of a land surface temperature (T_s) product from AMSR-E observations
- Evaluation at ground stations together with MODIS infrared T_s to highlight issues and difficulties of the inversions
- Overall, MODIS agrees better with the station T_s, but AMSR-E can provide 3 times more estimates

Correspondence to:
C. Jiménez,
carlos.jimenez@estellus.fr

Inversion of AMSR-E observations for land surface temperature estimation: 1. Methodology and evaluation with station temperature

C. Jiménez[1,2] ID**, C. Prigent[2]** ID**, S. L. Ermida[3]** ID**, and J.-L. Moncet[4]**

[1]Estellus, Paris, France, [2]LERMA, CNRS, Paris Observatory, Paris, France, [3]Instituto Dom Luiz, University of Lisbon, Lisbon, Portugal, [4]Atmospheric and Environmental Research, Inc., Lexington, Massachusetts, USA

Abstract Inversions of the Earth Observation Satellite (EOS) Advanced Microwave Scanning Radiometer (AMSR-E) brightness temperatures (T_{bs}) to derive the land surface temperature (T_s) are presented based on building a global transfer function by neural networks trained with AMSR-E T_{bs} and retrieved microwave T_s*. The only required inputs are the T_{bs} and monthly climatological emissivities, minimizing the dependence on ancillary data. The inversions are accompanied by a coarse estimation of retrieval uncertainty, an estimate of the quality of the retrieval, and a series of flags to signal difficult inversion situations. For ~75% of the land surface the root-mean-square difference (RMSD) between the training target T_s* and the neural network retrieved T_s is below 2.8 K. The RMSD when comparing with the Moderate Resolution Imaging Spectroradiometer (MODIS) clear-sky T_s is below 3.9 K for the same conditions. Over 10 ground stations, AMSR-E and MODIS T_s were compared with the in situ data. Overall, MODIS agrees better with the station T_s than AMSR-E (all-station mean RMSD of 2.4 K for MODIS and 4.0 for AMSR-E), but AMSR-E provides a larger number of T_s estimates by being able to measure under cloudy conditions, with an approximated ratio of 3 to 1 over the analyzed stations. At many stations the RMSD of the AMSR-E clear and cloudy sky are comparable, highlighting the ability of the microwave inversions to provide T_s under most atmospheric conditions. Closest agreement with the in situ T_s happens for stations with dense vegetation, where AMSR-E emissivity is less varying.

1. Introduction

Land surface skin temperature (T_s) is a critical variable in the interaction between the Earth surface and the atmosphere, with energy exchanges at the atmospheric boundary layer depending largely on the diurnal evolution of the T_s and its difference with the air temperature. While the latter is routinely observed at weather stations all around the globe, T_s is only measured at a very few stations with dedicated infrared radiometers to validate spaceborne T_s sensors [*Ermida et al.*, 2014; *Göttsche et al.*, 2016], at nondedicated sites that measure broadband thermal infrared radiation [e.g., *Augustine et al.*, 2005; *Stokes et al.*, 1994], or during specific measurement campaigns with similar radiometers (e.g., the Coordinated Enhanced Observing Period [*Koike*, 2004]).

T_s can be globally measured from satellites by infrared radiometers, with spatial and time resolutions depending on the platform orbit (geostationary or polar), but measurements can only be conducted under clear-sky conditions, and even under conditions classified as clear sky, they can be highly affected by residual cloud or aerosol (dust) contamination. The alternative for "all-weather" measurements are passive microwave radiometric observations, much less affected by clouds. Compared with the infrared observations, a larger dependence on the surface emissivity (the direct surface contribution to the T_{bs} is proportional to T_s and the emissivity), together with a larger variability of the emissivities related to a strong dependence on surface conditions make the T_s retrievals more challenging. Examples of surface conditions affecting the emissivity are the changes in soil humidity and vegetation water content and presence of snow and evolution of the air-ice-water phase in the snowpack. While infrared T_s operational products exist (e.g., the T_s products from Moderate Resolution Imaging Spectroradiometer (MODIS) [*Wan*, 2008] and from the Atmospheric Infrared Sounder [*Aumann et al.*, 2003], both aboard the Earth Observing System (EOS)-Aqua satellite since 2002, or the Satellite Application Facility on Land Surface Analysis (LSA SAF) T_s product from the Spinning Enhanced Visible and Infrared Imager (SEVIRI) on board Meteosat Second Generation (MSG) hh [*Trigo et al.*, 2011]),

there are still no T_s microwave products routinely available today. Together with the challenge of properly accounting for the emissivity variability in the retrieval, the inversion of microwave observations also has to face (1) emission emanating from subsurface layers for certain terrain conditions, or from vegetation canopy, i.e., not strictly a skin temperature; (2) a relatively coarse spatial resolution, related to the longer observation wavelengths, compared with the infrared; and (3) limited diurnal sampling as all current microwave radiometers are onboard polar orbiters, with only two overpasses per day, compared with the subhourly sampling from geostationary infrared sensors.

In a recent paper *Prigent et al.* [2016] presented a simplified methodology to retrieve T_s from brightness temperatures (T_{bs}) acquired by microwave connical scanners and applied the methodology to invert Special Sensor Microwave Imager (SSM/I) T_{bs}. This methodology used the experience gained by retrieving atmospheric and land surface parameters from the inversion method presented in *Aires et al.* [2001] and proposed a simplified scheme to minimize the number of ancillary inputs required in the processing. Given their objectives of building a climatological record of T_s and preparing for a potential near-real-time processing, a small number of auxiliary inputs was considered a priority in order to avoid discontinuity in the data record related to changes or absences of input sources, and to avoid waiting until the ancillary inputs are processed and disseminated. In essence, the proposed methodology consisted in training a neural network with a database of T_{bs} and T_s built from the detailed inversions of *Aires et al.* [2001] to provide a fast global transfer function approximating the T_{bs}-T_s relationship. The only required inputs (apart from the microwave T_{bs}) were precalculated microwave monthly mean emissivities available from the Tool to Estimate Land Surface Emissivity in the Microwave [*Aires et al.*, 2011]. Given the large impact of the land surface emissivity on the observed T_{bs}, adding emissivity estimates helps to constrain the inversion problem. Although instantaneous emissivities at the observation time will result in more accurate retrievals for locations with large emissivity variability, climatological estimates were found to be a good compromise for this simplified methodology.

The EOS-Aqua satellite was launched in May 2002 carrying multiple instruments, including Advanced Microwave Scanning Radiometer–EOS (AMSR-E), developed and provided by the Japan Aerospace Exploration Agency. It measured horizontally and vertically polarized T_{bs} at 6.9, 10.65, 18.7, 23.8, 36.5, and 89.0 GHz, scanning conically at a nominal incident angle of 55°. Spatial resolution of the individual measurements varied from 6×4 km at 89.0 GHz to 74×43 km at 6.9 GHz. The equator crossing time (local time) of their descending (ascending) node was 1:30 A.M. (P.M.). A swath width of 1450 km provided a revisiting time of 1–2 days. AMSR-E was operational from 2002 to 2011. Its successor, AMSR2, on board the Global Change Observation Mission-Water "SHIZUKU" (GCOM-W1) satellite was launched in May 2012, and it is currently operating with all AMSR-E channels available and a slightly better radiometric sensitivity and ground resolution (e.g., 5×3 km for the 89.0 GHz channels).

The close to midday and midnight AMSR-E and AMSR2 overpasses nicely complement the early morning and late afternoon overpasses of the SSM/I and Special Sensor Microwave Imager Sounder (SSMIS) instruments, resulting in a typical sampling of the T_s diurnal cycle at four distinct times of the day. In an effort to prepare a common inversion of these sensors T_{bs}, we apply a similar methodology to *Prigent et al.* [2016] to retrieve T_s from the AMSR-E observations and evaluate the produced estimates at a number of ground stations. The paper is organized as follows: first, the methodology to invert the AMSR-E observations and the data used to evaluate the retrieved T_s are presented. This is followed by characterizing the AMSR-E inversions, and an evaluation of the produced T_s at a selection of ground stations. Further evaluation at the global scale with coincident satellite infrared T_s estimates is presented in a companion paper (Part 2). Finally, the paper is summarized, and paths for further improvements of the methodology are discussed.

2. Methods and Data

2.1. Inversion Methodology

The AMSR-E T_{bs} are inverted with the methodology presented in *Prigent et al.* [2016], with some minor adaptations to deal specifically with the AMSR-E observations. Similar to the SSM/I inversions presented in *Prigent et al.* [2016] work, a neural network is trained with a database of coincident AMSR-E T_{bs}, retrieved T_s from the 2003 AMSR-E inversions presented in *Lipton et al.* [2015] (referred to as T_s*), and a monthly AMSR-E emissivity climatology derived using as ancillary T_s data from MODIS on the same Aqua spacecraft [*Moncet et al.*, 2011]. As for the SSM/I inversions, a strategy of having separate neural networks for (1) Greenland and Antarctic, referred to as permanent snow, and (2) the remaining continental land is also adopted. Unlike SSM/I,

inversion tests showed that independent trainings for the nighttime and daytime retrievals were more effective at approximating the T_{bs}-T_s relationship. The AMSR-E close to midnight and midday overpasses typically result in quite different surface-atmosphere conditions with a more different range of T_s (compared with the closer conditions between the SSM/I early morning and late afternoon overpasses), and an inversion having two dedicated setups (one for nighttime and one for daytime) for each of the two geographical selections was adopted.

Multilayer perceptrons are used to implement each neural network. The input layer has as many nodes as the number of frequency channels and associated emissivities used for the inversion. It is followed by a hidden layer of 10 nodes, and the output layer with one node for the retrieved T_s. For the training, 10^5 cases are randomly selected from the T_{bs}-T_s database. The initial weights of the neural network are randomly initialized by the Nguyen-Widrow algorithm [*Nguyen and Widrow*, 1990], and the final weights are assigned by a Marquardt-Levenberg backpropagation algorithm [*Hagan and Menhaj*, 1994]. To prevent overfitting to the training data set, a cross-validation technique is used to monitor the evolution of the training error function.

Once the neural network is trained, it becomes a transfer function to produce T_s from the observed T_{bs} and associated emissivities. As training the neural network means minimizing an error function, here the sum of square errors of the difference between the neural network response to the training input vector and the corresponding target vector, if the initial weights are slightly changed, the minimization of the error function results in a new set of final weights and corresponding transfer function. In most cases the resulting transfer functions are very close, and for well-constrained inversion situations the variability in the output (here the retrieved T_s) by applying the neural networks from different trainings is small. Likewise, a large variability is an indication of inversion situations where the neural network has difficulties to solve the inverse problem. To use this variability as a form of quality control for the inversions, 50 neural networks for each of the four retrieval setups (continental land and permanent snow, each with daytime and nighttime separated inversions) are trained with different initial conditions. The neural network with the smallest training error is selected to produce the retrieved T_s, and the variability of the 50 final T_s for each inversion is monitored to capture cases where the inversion situation seems problematic.

The AMSR-E 18.7, 36.5, and 89.0 GHz vertically and horizontally polarized channels and the 23.8 GHz vertically polarized channel are used for the retrieval, in a similar configuration to the SSM/I retrievals of *Prigent et al.* [2016]. In principle the 6.9 and 10.6 GHz lower frequency channels could also have been considered for the retrieval. They are more transparent to clouds, but their spatial resolution is coarser, they sample a deeper surface layer, and they are more sensitive to surface characteristics, requiring a more accurate estimate of the surface emissivity to derive T_s. In addition, they are known to suffer from radio frequency interference [*Li et al.*, 2004]. The spatial resolution of the 6.9 GHz channels is approximately 3 times coarser than at 18.7 GHz channels, so we did not consider it any further as we attempt to produce T_s retrievals at a relatively fine spatial resolution. The 10.6 GHz channels are closer in spatial resolution to the 18.7 GHz channels, but inversion tests with the training database did not show any improvement in performance when these channels were added to the higher-frequency channels. With our inversion methodology relying on monthly climatological emissivity, it is possible that any positive effects on the inversion related to a larger transparency to clouds are compensated by unaccounted variability of the surface emissivity at this frequency. Therefore, we favored the channel selection without the 10.6 GHz in order to have an inversion algorithm as close as possible to the SSM/I inversions.

An estimate of retrieval uncertainty is always useful and required for some applications (e.g., in data assimilation), and a simple uncertainty map has been derived by analyzing the total retrieval errors in the training database. The selected final neural network is applied to a new subset of the training database not seen by the neural network during the training phase, and the differences between the target surface temperature in the database T_s* and the retrieved T_s are used to infer an uncertainty estimate for a range of emissivity and T_s values. The result is a lookup table storing the mean difference for 56 combinations of T_s and emissivity, using the 18.7 GHz horizontally polarized channel. This emissivity has a slightly larger variability than the other emissivities, so it is well indicated to classify diverse inversion situations. For a given retrieval of T_s and associated emissivity, the lookup table is searched and the found value is used as a simple estimation of the inversion uncertainty. It should be stressed that the uncertainty is derived from the difference with the microwave T_s of the training database, but not with the unavailable real ground T_s corresponding to the database T_{bs}.

Table 1. Station Location, Climate, and Surface Type

ID (Longitude, Latitude)	Location	Climate	Surface
	Temperate		
EVO (−8.00, 38.5)	Evora, Portugal	Mediterranean	Forest
GCM (−89.9, 34.2)	Goodwin Creek, Mississippi, USA	Humid subtropical	Forest
BND (−88.4, 40.0)	Bondville, Illinois, USA	Humid continental	Cropland
	Boreal		
PSU (−77.9, 40.7)	Pennsylvania State University, Pennsylvania, USA	Humid continental	Forest, croplands
SFA (−96.6, 43.7)	Sioux Falls, South Dakota, USA	Humid continental	Cropland
FPK (−105.1, 48.3)	Fort Peck, Montana, USA	Semiarid	Croplands
	Subtropical		
DRA (−116.0, 36.6)	Desert Rock, Nevada, USA	Arid	Rock
GBB (−89.9, 34.2)	Gobabeb, Namib Desert, Namibia	Arid	Rock, sand
KAL (18.3, −23.0)	Kalahari, Namibia	Arid	Rock
	Highlands		
TBL (−105.2, 40.1)	Table Mountain, Boulder, Colorado, USA	Highland	Rock, shrub

As the microwave T_s^* in the training database is the product of an inversion subject to retrieval errors (see *Aires et al.* [2001] for a discussion), the uncertainty from the derived lookup table should be consider as a lower estimate of the "true" retrieval error.

2.2. Data Sets

The AMSR-E T_{bs} were extracted from the National Snow and Ice Data Center archive [*Shcroft and Wentz*, 2013]. During the inversions, the 18.7, 23.8, and 36.5 GHz channels are applied at their original resolutions (27×16, 31×18, and 14×8 km, respectively), while the 89.0 GHz channels with a original resolution of 6×4 km are resampled to the 36.5 GHz resolution. An alternative would have been to select the T_{bs} with their footprints matched to the 18.7 GHz (the channel with the lowest resolution). *Prigent et al.* [2016] presented correlation analyses showing that the 19.3 GHz channel contributes the least to the T_s retrieval, and the same was found when repeating the analysis with the AMSR-E 18.7 GHz channel and our inversion database. Therefore, we prefer not to degrade all channel resolutions to the 18.7 GHz footprint. The highest resolution channels are likely to have more weight on the retrieval at most locations, potentially resulting in a T_s retrieval with an "effective" spatial mean resolution closer to 12 km (36.5 GHz) than to 21 km (18.7 GHz). According to this, the T_s retrieval is placed in the 14×8 km swath grid of the 36.5 GHz channel, although information from a larger footprint is likely to affect the retrieval.

To evaluate the AMSR-E inversions, data records of T_s estimated from ground infrared measurements at 10 stations in the year 2010 were available from an evaluation data set compiled by the European Space Agency (ESA) GlobTemperature Data User Element (DUE) project (http:www.globtemperature.info). The stations are listed in Table 1, grouped by climate types. Three of them (EVO, GBB, and KAL) are run by the Land Surface Analysis Satellite Applications Facility (LSA SAF) [*Trigo et al.*, 2011] and have narrowband infrared radiometers dedicated to the validation of satellite T_s. The remaining seven (GCM, BND, PSU, SFA, FPK, DRA, and TBL) belong to the Surface Radiation Network (SURFRAD) [*Augustine et al.*, 2005] and use broadband infrared radiometers that are part of a suite of different instruments dedicated to measure radiation-related variables. Notice that apart from the difference in radiometers, the data at the stations are not identically processed. For the SURFRAD stations, the emissivity required to derive the T_s from the radiometric observations comes from the database of *Seemann et al.* [2008]. For the LSA SAF stations, EVO and KAL use the emissivity retrieved for the LSA SAF satellite T_s inversions [*Trigo et al.*, 2008], while the emissivity at GBB is estimated following *Göttsche and Hulley* [2012]. Notice that for EVO, apart from the radiometers measuring the upwelling and downwelling radiation, there is a third radiometer measuring canopy T_b, which is combined with the other measurements assuming a fixed fraction of vegetation cover [*Ermida et al.*, 2014]. Together with the T_s estimates, an estimation of T_s uncertainty is provided by error propagating the broadband emissivity uncertainty and the measurement uncertainty of the radiances [*Göttsche et al.*, 2016]. The resulting overall T_s uncertainty lies in a range between 0.6 and 2 K for all stations [*Martin and Goöttsche*, 2015].
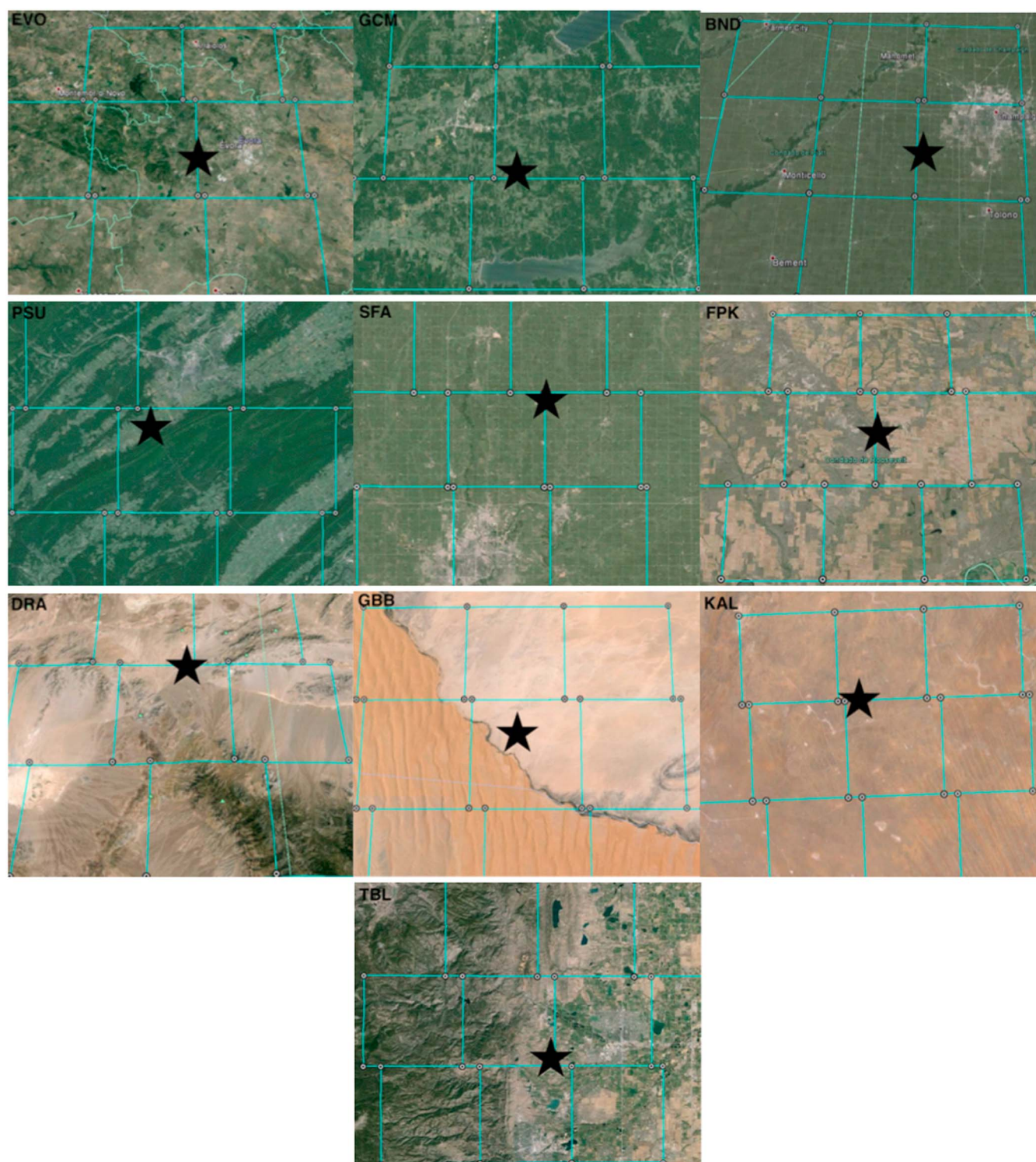
Figure 1. Aerial photos of the area surrounding the 10 stations listed in Table 1. The position of the stations is marked by the black stars. The blue squares have a dimension of 12×12 km and are placed to give an approximated idea of the AMSR-E T_s spatial resolution (12 km is the spatial mean resolution of the AMSR-E swath grid adopted for the T_s retrievals). Photos courtesy of Google Earth[TM] mapping service.

The stations are associated with different environments and were accordingly organized into four main climate types: temperate, boreal, subtropical, and highlands. Aerial photos of the stations are shown in Figure 1 and are used to judge the spatial homogeneity around the station. The stations EVO, GCM, and BND are located in temperate climate areas; the EVO station presents a drier Mediterranean climate, and the remaining ones belong to more humid environments. The stations PSU, SFA, and FPK have boreal climates; PSU and SFA are typical of humid environments, while FPK represents a very dry environment. DRA, GBB, and KAL are desert stations, characteristic of the subtropical climate. The last station, TBL, although belonging to a temperate climate, is located in a mountainous region; because of the high spatial heterogeneity, this station is analyzed separately. For each station, AMSR-E overpasses are matched to the station available T_s observations allowing a maximum distance of 7 km between the station location and the pixel center, and a maximum difference of 5 min between the AMSR-E and the station time acquisitions. As the station data are recorded every minute and the records are quite continuous, in practical terms, quite continuous, the time difference is in most cases within one minute.

To provide a satellite infrared reference to the AMSR-E evaluations, MODIS T_s (MYD11A1, collection 5) [*Wan and Li*, 2008] is also compared to the station data. MODIS-Aqua and AMSR-E are on board the same satellite platform, so they are closely collocated in time. Regarding the spatial matching, MODIS 1 km data were averaged to the 14×8 km swath grid adopted for the AMSR-E T_s retrieval to assure that surface heterogeneity impacts equally both T_s estimations. Only MODIS pixels with the best quality flag were considered. Grid cells where less than 100% of MODIS pixels are valid are considered as cloudy, and the resulting cloud mask is used to separate AMSR-E estimates into clear and cloudy sky. The original 1 km MODIS product is also compared at some stations, with changes in the agreement with the station between the MODIS 1 km T_s and the AMSR-E resolution MODIS T_s used as a coarse indicator of surface heterogeneity (i.e., better agreement at 1 km implying than the station conditions are more representative at the MODIS original resolution than the much coarser AMSR-E resolution).

3. Inversions Characterization

Following the methodology described in section 2.1, inversions of AMSR-E T_{bs} have been conducted at the sensor ground location. As discussed in section 2.2, the retrievals are conducted in the AMSR-E swath grid of 14×8 km of the 36.5 GHz channel, but the retrievals are also affected by observations with coarser resolution from the lower frequency channels. Spatial coverage is global, twice a day at ~1:30 A.M./P.M., but the 1–2 days revisiting time and some missing AMSR-E acquisitions result in gaps in the data record.

The inversions corresponding to 4 days in 2008 are presented in Figure 2 as an example of retrieved T_s. With the 1–2 days revisiting time, full coverage only happens at the higher northern and southern latitudes. Missing nighttime orbits over the night are also noticeable for this specific days. The expected T_s geographical patterns are well reproduced, with the warm and cold regions associated with the different climate regions clearly visible in the maps. The nighttime/daytime differences are also as expected, with the largest gradients occurring over arid and semiarid areas. More detailed discussions are provided below.

3.1. AMSR-E Retrieval Uncertainty

The ability of the neural network to approximate the T_{bs}-T_s relationship under different inversion situations is shown in Figure 3 (black lines). The figure shows histograms of the nighttime/daytime difference between the microwave T_s* (the target variable during the neural network training) and the retrieved T_s (the output from the neural network once it is trained) for three ranges of the 18.7 GHz horizontally polarized emissivity and two ranges of T_s. As described in section 2.1, this difference is used to build a lookup table to produce an approximated uncertainty characterization for the T_s retrievals. Global maps of this retrieval uncertainty are plotted in Figure 4 for 4 days in 2008. Root-mean-square differences (RMSDs) ranging from 2.0 K (warm T_s, high emissivity) to 4.0 K (cold T_s, low emissivity) are shown in Figure 3, with the RMSD below 2.8 K for ~75% of the global land surface. Large uncertainty can be observed for snow-covered and humid surfaces, conditions where the climatological emissivities can be poorly representing the true emissivity, implying larger difficulties in retrieving the surface T_s. This is also visible in Figure 4, where large uncertainty is estimated for the snow-covered regions. The smallest uncertainty occurs over tropical forests. This possibly reflects a better match between the climatological emissivity used in the inversion and the real emissivity. In these regions the surface is temporarily more stable and the relatively simple surface emission models used to derive the emissivity from the microwave observations are closer to reality. The opposite happens in snow-covered regions,
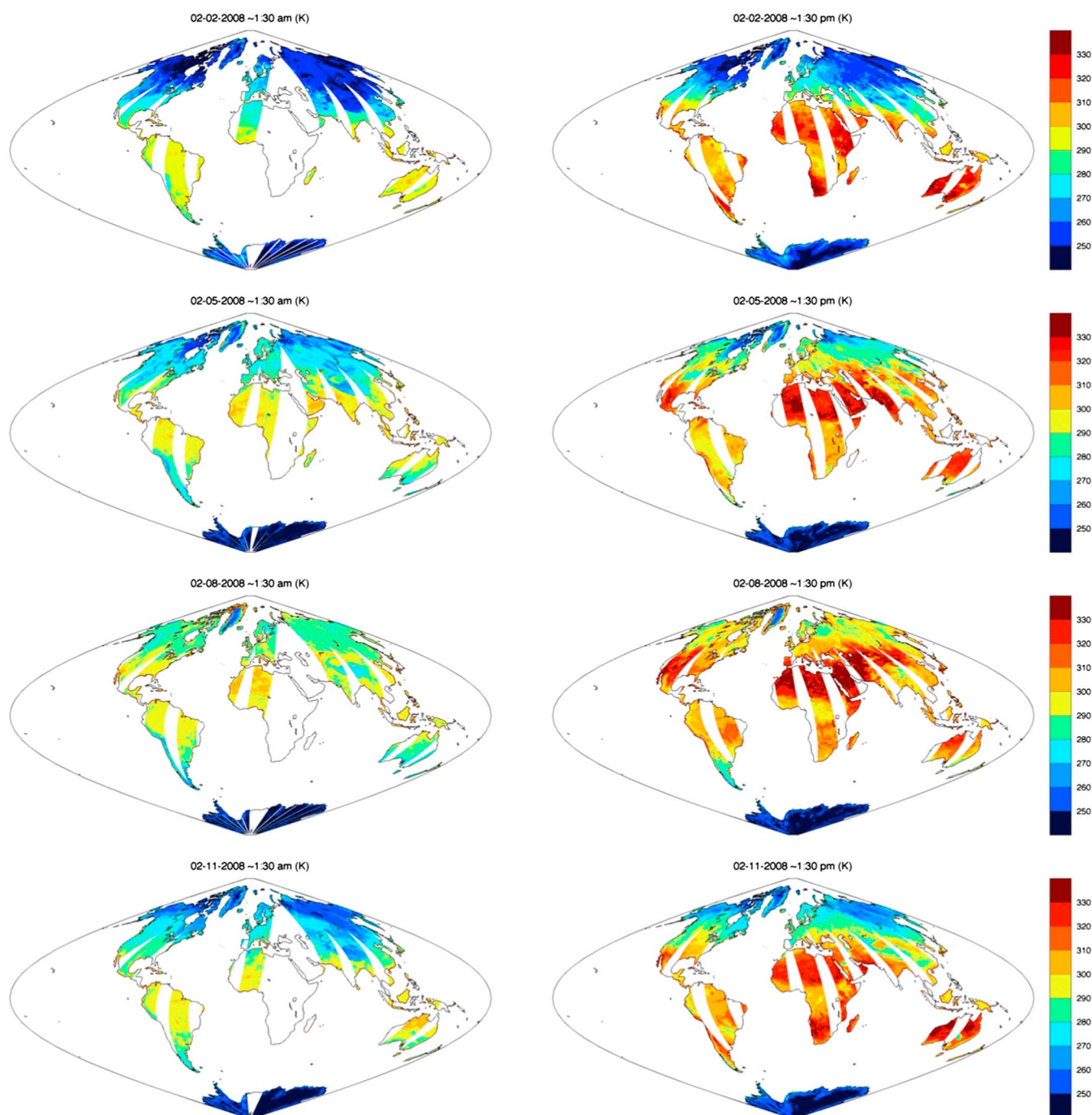
Figure 2. Example of AMSR-E retrieved T_s for 2 February, 2 May, 2 August, and 2 November 2008. (left column) nighttime overpass retrieval; (right column) the daytime overpass. The gaps over land correspond to areas where there are no AMSR-E data available for the inversions; most of them are due to the AMSR-E swath, but missing portion of orbits are also visible during the night.

where melting and snow metamorphisms result in a more varying emissivity and more difficulties to model the surface emission. For most cases the RMSD in Figure 3 is larger in the daytime than at night. This is likely to reflect the most challenging inversion situation for the daytime overpasses. Strongest subsurface thermal gradients are more likely at daytime and can accentuate the impact of microwave penetration in the retrieval (i.e., the T_s to be retrieved is not just a skin temperature but represents a temperature derived from the emission of a nonuniform temperature layer of a certain depth). Figure 4 also shows that in general the retrieval uncertainty is lower at night than in the daytime.
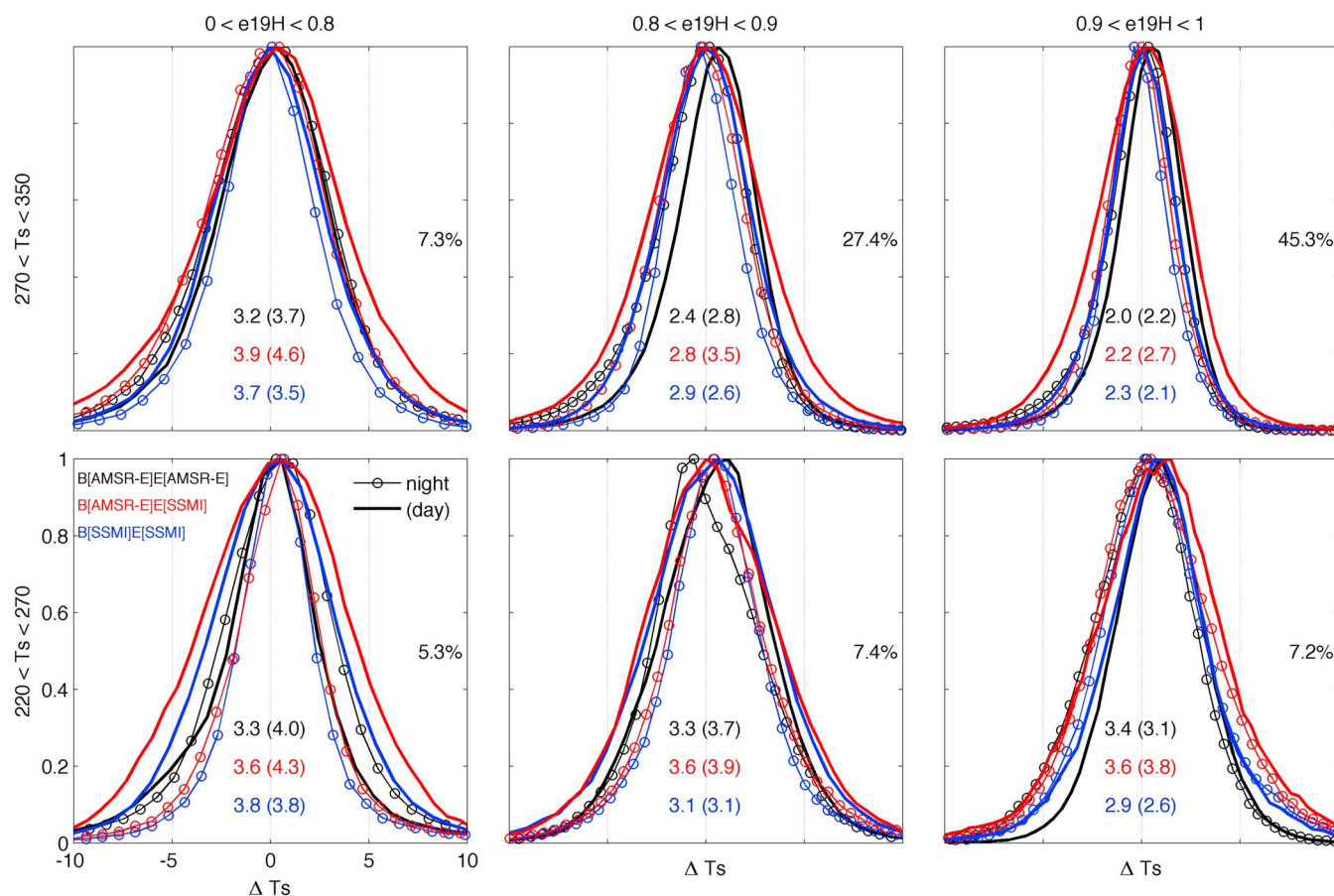
Figure 3. Histograms of the difference between the retrieved T_s from the neural network inversion and the original microwave T_s^* (ΔT_s). The differences are plotted for two T_s ranges (top to bottom) and three 18.7 GHz horizontally polarized emissivity ranges (left to right). AMSR-E inversions using AMSR-E emissivities are plotted in black; AMSR-E inversions using SSM/I emissivities are plotted in red; SSM/I inversions using SSM/I emissivities are plotted in blue. Open circles represent the nighttime overpass inversions, and solid lines represent the daytime. The numbers in the middle give the RMSD for each combination and overpass (daytime in brackets). The numbers on the right give the percentage of cases in the global training database for each emissivity and T_s combination.

3.2. SSM/I Retrieval Uncertainty

For reference, Figure 3 also shows the T_s uncertainty characterization when SSM/I T_{bs} are inverted using the SSM/I retrieval scheme presented in *Prigent et al.* [2016] (i.e., similar retrieval algorithm but trained with a database of SSM/I T_{bs} and corresponding T_s^*). The histograms (blue lines) are comparable to the AMSR-E inversions presented here, with RMSD ranging from 2.1 to 3.8 K. For these inversions, nighttime and daytime denote the early morning and late afternoon overpasses of SSM/I. As discussed in section 2.1 the differences between those surface-atmosphere conditions are smaller than for the AMSR-E overpasses, and the RMSDs for nighttime/daytime are closer than for AMSR-E. Overall, these figures suggest that inversions with comparable uncertainty are possible from the SSM/I/SSMIS and AMSR-E/AMSR2 sensors, which is a good outcome for a future product that combines estimates from all sensors.

3.3. Inversion With SSM/I Emissivity

A future joint SSM/I/SSMIS and AMSR-E/AMSR2 inversion is planned, and for those inversions, using a common emissivity climatology may help reduce differences in the retrieved T_s related to differences in the estimated emissivities. Compared with AMSR-E, some of the SSM/I(SSMIS) channels are centered at slightly different frequencies, but the frequency dependence of the emissivity is rather limited and not likely to bring any significant differences in the monthly emissivity from the different sensors [*Prigent et al.*, 2008]. Most significant can be the differences caused by the coarser spatial resolution of SSM/I (AMSR-E roughly improving the SSM/I spatial resolution by a factor of 2), specially for regions with large surface heterogeneity.

To test the impact of using SSM/I emissivities, inversions of AMSR-E T_{bs} were conducted using the methodology described in section 2.1, but replacing the AMSR-E emissivities with the same SSM/I climatological
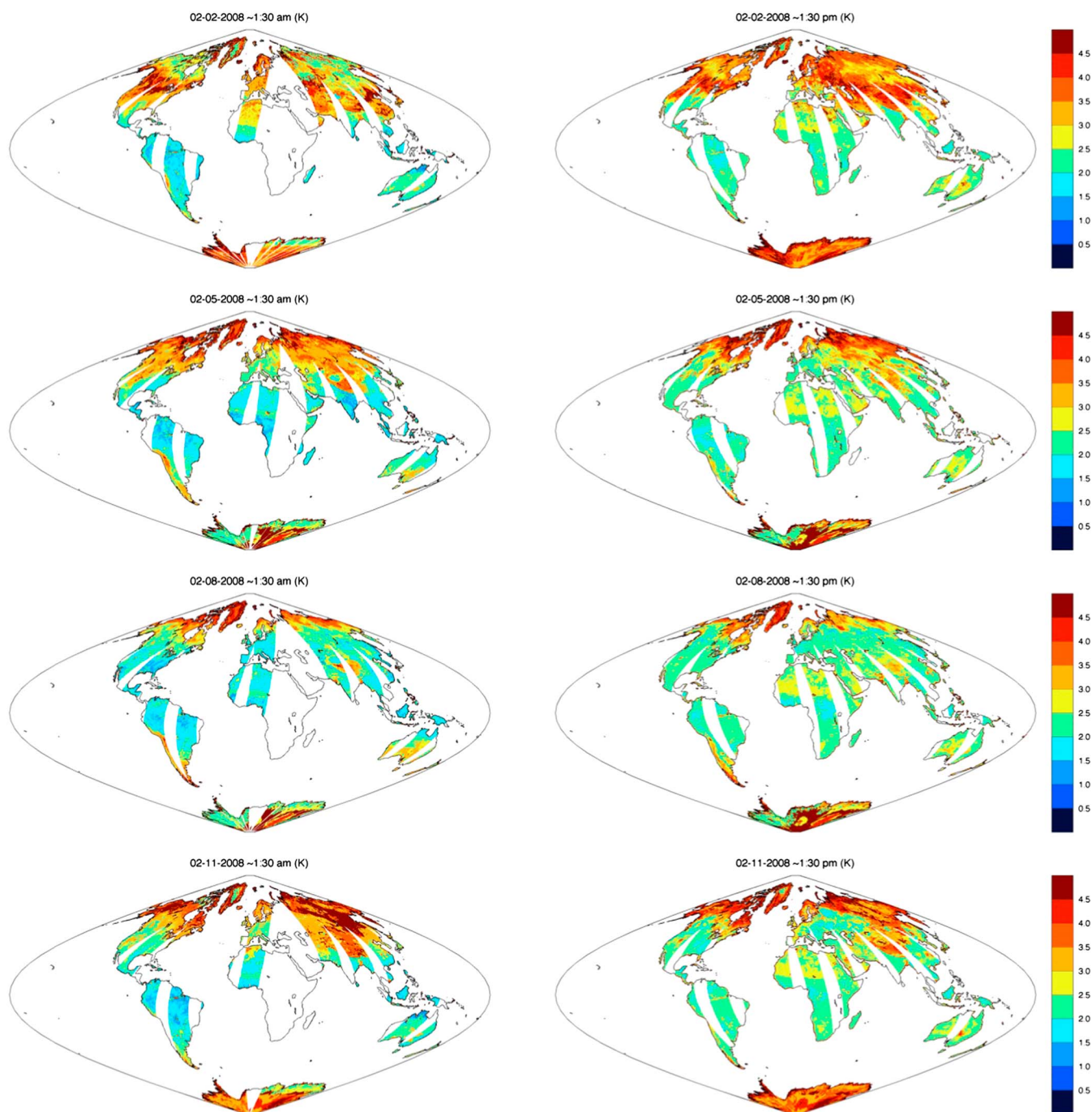
Figure 4. As in Figure 2 but showing the retrieval error.

emissivity as in *Prigent et al.* [2016]. Figure 3 (red lines) shows the same histograms as before, but this time for the AMSR-E (T_{bs}) and SSM/I (emissivity) inversions. RMSDs are only slightly larger than for the all (T_{bs} and emissivity) AMSR-E inversions, ranging from 2.2 to 4.6 K instead of 2.0 to 4.0 K, suggesting that using a common climatology for the SSM/I(SSMIS) and AMSR-E inversions could be considered.

3.4. Differences With MODIS T_s

A true T_s to evaluate the retrieval uncertainty at the global scale of the AMSR-E inversions does not exist. But a comparison with another T_s product could also be useful under the assumption that these new T_s estimates are a reasonable representation of the unknown true T_s. This is illustrated in Figure 5, where histograms of the difference between the original AMSR-E T_s* from the training database and collocated MODIS T_s
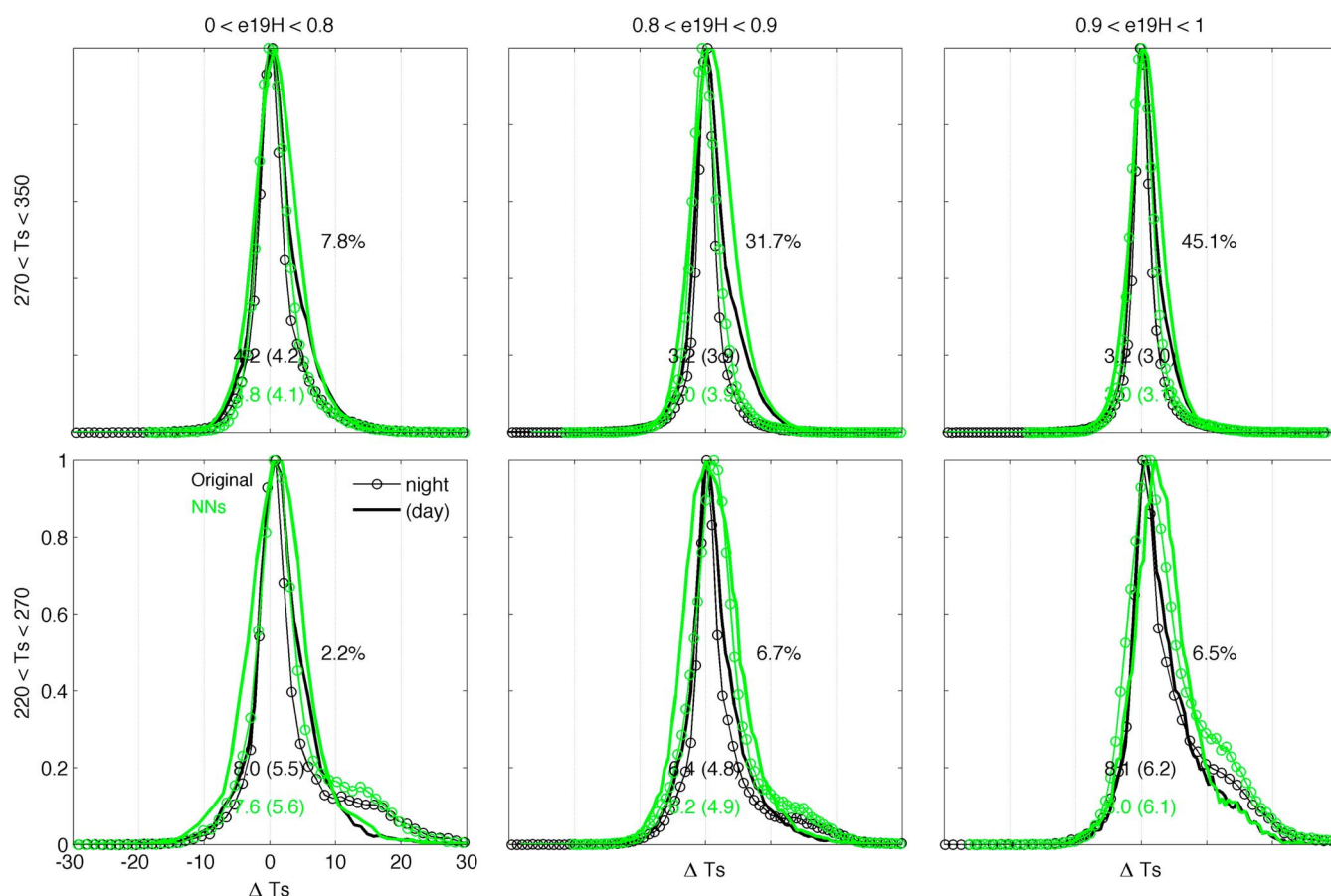
Figure 5. Similar to Figure 3 but showing histograms of the difference between the MODIS T_s and (1) the original microwave T_s^* (black lines) and (2) the T_s from the neural network inversion (green lines).

(black lines) are compared with histograms of the difference between the neural network retrieved T_s and the MODIS T_s (green lines). The RMSD are close for both differences (original AMSR-E retrieval and our neural network scheme), indicating that the new AMSR-E inversion methodology trained on the original AMSR-E inversions do not notably degrade the level of agreement with the infrared T_s estimates from MODIS. For ~75% of the global land surface, RMSD are below 3.9 K. A much more detailed comparison of the AMSR-E and MODIS T_s is presented in Part 2.

3.5. Retrieval Variability

The retrieval variability defined as the standard deviation of the estimates at each pixel from the multineural network retrievals (see section 2.1 for the details) is displayed in Figure 6 for 4 days in 2008. For a large part of the globe the variability is below 1.5 K but can show larger values specially over some arid and snow-covered areas. For instance, in Northern Africa the locations with sand dunes are clearly associated with a larger variability, indicating the difficulties of the inversion in regions with large penetration depth and emission emanating from subsurface layers.

The retrieval variability increases for locations where we expect inversion difficulties. In most cases, they correspond to areas where the emissivity applied in the retrieval can be poorly representing the true conditions. This is the case for snow-covered areas and humid surfaces, as discussed in section 3.1. For coastal regions the situation is similar, with very low emissivities if water is present in the swath position of the AMSR-E observation, which are not always properly captured by the closest emissivity estimate selected from the climatology. Convection activity in the overlying atmosphere can also result in difficult inversions. In this case, the problem is impact of the hydrometeors (rain and clouds) in the brightness temperatures of the different frequency channels, which is not quantified by the retrieval as the inversion assumes that most of the microwave emission comes from the surface.
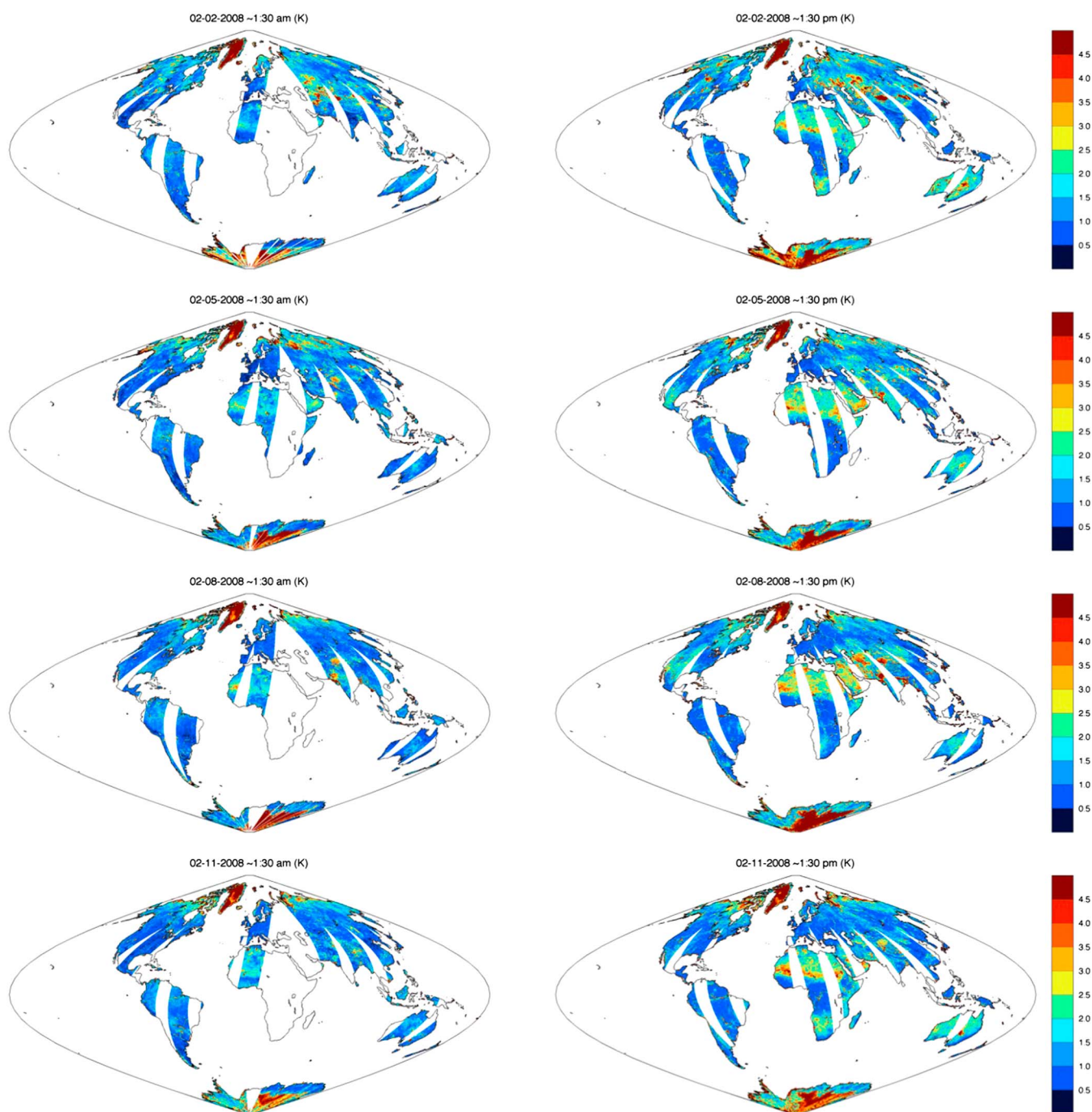
Figure 6. As in Figure 2 but showing the retrieval variability.

To help identify these situations, a series of flags have been added to the retrieval product. The flags signal (a) snow-covered pixels, using the snow water equivalent (SWE) product from GlobSnow [*Takala et al.*, 2011]; (b) inundated pixels, using a monthly climatology from the Global Inundation Extension from Multi-Satellites (GIEMS) [*Prigent et al.*, 2012]; (c) coastal pixels; (d) pixels with large microwave penetration depth, using a monthly climatology of radar backscattering from [*Prigent*, 2005]; and (e) pixels with atmospheric convection activity, by looking at T_b depressions in the 89.0 GHz channels caused by ice clouds. Figure 7 (top) shows for 2 May 2008 the retrieval variability for the pixels flagged for different conditions (the median of the variability
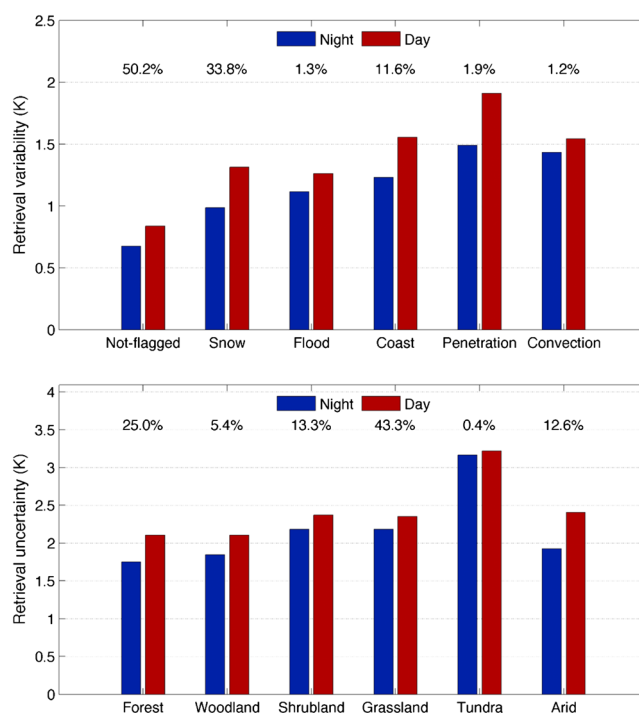
Figure 7. Statistics of the AMSR-E inversion for 2 May 2008. (top) The retrieval variability for different conditions: pixels identified as being snow covered (snow), close to the coastal line (coast), with convection activity in the overlying atmosphere (convection), with the thermal radiation likely emanating from deep layers within the underlying soil (penetration), with a large possibility of being flooded (flood), and for the remaining pixels (not flagged). The bars display the median of the retrieval variability of the individual pixels for each surface condition (blue for nighttime inversions, red for daytime inversions). The numbers above the bars indicate the percentage of pixels corresponding to a given surface condition. (bottom) Similar to Figure 7 (top) but giving the retrieval error for the not-flagged pixels classified as a function of land cover.

of all pixels for a given condition), and for the nonflagged pixels, together with the percentage of pixels for each condition. For the nonflagged pixels nighttime and daytime variability are well below 1.0 K, while for the flagged pixels it is above 1.0 K, with the largest variability for the pixels with large penetration depth.

Figure 7 (bottom) also shows the retrieval uncertainty presented in section 3.1 for different biome types (the median of the uncertainty of all pixels for a given biome, only including the nonflagged pixels). The uncertainty is around 2.0 K for all biomes apart from the tundra, where it reaches over 3.0 K. The tundra biome has a very small number of pixels (most of them were flagged as snow covered). Some of those pixels can still be snow contaminated (even if not detected by the snow product) or can correspond to very wet areas with abundance of water streams during the warm season, in both cases having the typical large uncertainty associated with cold and low emissivity conditions (see Figure 3). The smallest uncertainty corresponds to the forest and woodlands, with quite stable surface conditions and the emissivity climatology likely capturing the true emissivity and constraining well the inversion problem. It is worth noticing that the arid regions also have comparable uncertainty once pixels with possible microwave penetration are removed. Still, some specific difficulties may be encountered for situations where changes in moisture and vegetation are not well captured by the monthly climatology.

4. Evaluation With In Situ Measurements

An evaluation of the AMSR-E inversions at the 10 stations listed in Table 1 is presented here. For reference, a comparison with MODIS T_s is also included. As main statistics, the bias (mean of the difference between the satellite and the in situ T_s), the standard deviation of the same difference (STD), and the RMSD are calculated for the AMSR-E and MODIS differences, for clear-sky (MODIS and AMSR-E) and cloudy-sky (AMSR-E), and for nighttime/daytime separately.
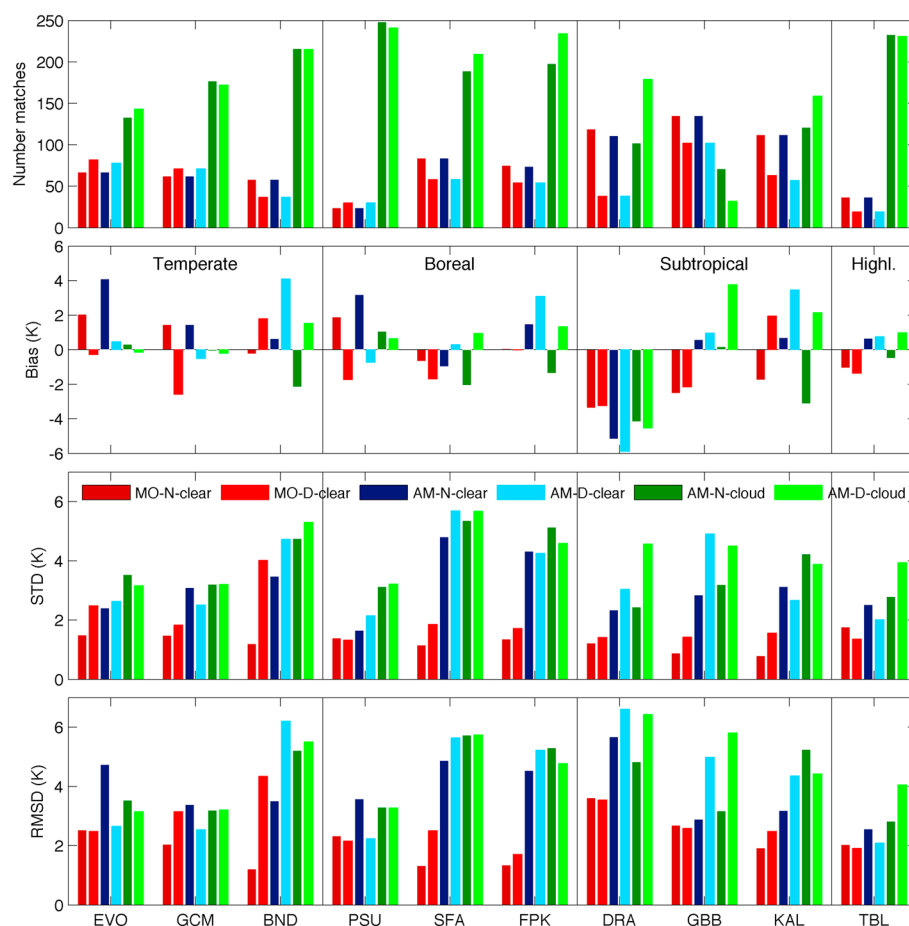
Figure 8. Statistics of the 2010 comparison of MODIS and AMSR-E T_s with in situ measurements at 10 stations. From top to bottom: (1) Number of matches between satellite and in situ T_s; (2) bias, average of the difference between satellite and in situ T_s; (3) STD, standard deviation of the difference; and (4) RMSD, root-mean-square of the difference. For each station there are six bars corresponding to clear-sky MODIS (MO, red) nighttime (N, dark color) and daytime (D, light color), and AMSR-E (AM, blue and green) nighttime/daytime and clear (blue)/cloudy (green) sky.

4.1. Annual Evaluation

The statistics of the 2010 full year comparison are summarized in Figure 8, together with the number of matches for each situation (daytime/nighttime, clear/cloudy sky). At most stations nighttime/daytime conditions are closely sampled in terms of number of cases; an exception is the arid DRA station, where the number of nighttime cases is more than double the number of daytime cases due to the quality filtering of MODIS data at this specific location. Over these stations the number of cloudy-sky cases is in general much larger than the clear-sky cases (clear-sky cases identified with the cloud mask discussed in section 2.2); the only exception is the arid GBB station. The ratio of available AMSR-E matched MODIS T_s estimates to AMSR-E T_s estimates is ~0.3. This highlights the importance of having T_s products that can provide estimates also for cloudy conditions.

The overall picture given by the annual biases does not show a clear direction (positive or negative) in terms of daytime/nighttime, clear-/cloudy-sky, climate group, or sensor is not obvious. An exception is the DRA station, where both MODIS and AMSR-E have large negative biases for all situations. At many stations the RMSD of the AMSR-E clear sky and cloudy sky are comparable, highlighting the ability of the microwave inversions to provide T_s estimates under most atmospheric conditions. The AMSR-E all-stations mean RMSD for clear sky is 4.0 K, and only slightly larger for cloudy sky at 4.3 K. Comparing the MODIS and AMSR-E STD for clear-sky conditions, for all stations the MODIS STD is smaller than the AMSR-E STD. The same happens for the RMSD, with an all-stations mean RMSD of 2.4 K for MODIS, lower than the 4.0 K for AMSR-E.

Closer RMSD for MODIS and AMSR-E is observed for the temperate stations, compared with most of the boreal and subtropical stations. The microwave emissivity is less seasonally varying than at other stations

(e.g., EVO and GCM are less affected by snow episodes), and the presence of vegetation at these locations reduces the issues with microwave penetration, likely resulting in less uncertain inversions. For the EVO station, AMSR-E and MODIS presents a high positive bias for nighttime clear-sky observations, in accordance with previous studies for MODIS and SEVIRI for the same location [*Trigo et al.*, 2008]. There is also a degradation of MODIS nighttime bias from 1.5 K at the original resolution to 2.0 K at the AMSR-E resolution, suggesting that the station representativeness degrades with distance to the station, particularly during the night. This nighttime/daytime variation of the bias is also present at the GCM and BND station.

Compared with MODIS, AMSR-E presents a much larger RMSD at the boreal stations. The large differences are mainly associated with very low T_s values when the surface is likely to be covered with ice or snow. If only in situ T_s observations above 274 K are considered, the overall AMSR-E STD of 3.1/5.6/4.6 K at PSU/SFA/FPK stations decreases to 2.7/3.9/3.8 K. At the PSU station, there is again a contrasting bias from daytime to nighttime for the clear-sky comparisons, which is consistent between AMSR-E and MODIS. The PSU station is located in an agricultural area that is surrounded by forests; trees tend to have higher (lower) temperatures than the surface during nighttime (daytime) resulting in higher (lower) remotely sensed T_s values, in agreement with the positive (negative) bias observed. A change in the MODIS bias when using the closest 1 km pixel or the resampled MODIS T_s also points to discrepancies in the point versus area-integrated T_s (from −0.3 to 0.8 K). The SAF and FPK stations are located in more homogeneous cultivated areas but still subject to snow coverage in the winter period resulting in difficulties for the AMSR-E inversions.

The three subtropical stations discussed here are representative of arid conditions. For these stations the larger AMSR-E RMSD compared with MODIS is related to these regions being prone to large microwave penetration depth (i.e., the skin temperature at the station can be different from the subsurface-integrated microwave temperature). The DRA station is located in an area of very irregular surface relief, and both MODIS and AMSR-E compare very poorly with the in situ measurements. MODIS bias presents a large degradation in the statistics from the original 1 km resolution to the AMSR-E resolution, especially for daytime, which supports the negative impact of a high surface heterogeneity on the T_s comparison. For the GBB station, there is a high AMSR-E bias for daytime cloudy sky. This station is located over rocky terrain but there are sand dunes at a distance of ∼2.5 km from the station, which can be part of the AMSR-E pixel and negatively impact the comparison due to the expected microwave emission from subsurface layers. At the KAL station, there is also a high contrast between daytime and nighttime AMSR-E bias values, which is also occurring for MODIS. MODIS daytime bias values also present a degradation from 0.9 K at the 1 km resolution to 2.0 K at the AMSR-E resolution, which suggests again representativity issues between the in situ and satellite spatial scales.

The highland station TBL is located in a very heterogeneous region both in terms of orography (being close to a mountain range) and of vegetation cover. Nevertheless, at this station the agreement of MODIS and AMSR-E is relatively good compared with the other stations.

In summary, MODIS agrees better with the stations measurements than AMSR-E. This can be expected due to the fact that both MODIS and the station instruments measure infrared radiation, while AMSR-E operates in the microwave; i.e., MODIS and the station measure a skin temperature, while AMSR-E observes a depth-integrated temperature, which can be different if the are subsurface thermal gradients at the depths where the microwave observations are sensitive. The larger microwave emissivity variability can also play a role given the satellite area-integrated to station point-observation disparity. The area surrounding the station is likely to be thermally more heterogeneous in the microwave given the smaller dependence of the infrared radiation on the emissivity and a generally more stable infrared emissivity. Nevertheless, the differences in RMSD are significantly large at some stations, pointing also to difficulties in the AMSR-E inversions.

4.2. Seasonal Evaluation

Seasonal changes in the differences with the T_s station were observed at the DRA, EVO, and GCM stations. Figure 9 illustrates this behavior for the two temperate stations by plotting the seasonal bias of MODIS (clear sky) and AMSR-E (all weather). At the EVO station (Figure 9, top) there are nighttime and daytime seasonal changes in the AMSR-E bias, although it is more pronounced for nighttime. The bias is negative in winter (January-February-March), and positive in summer (July-August-September). MODIS also presents a negative daytime bias in winter and positive in summer (although very small for summer). In contrast, the nighttime MODIS bias is positive for all seasons with close values. At the GCM station (Figure 9, bottom), at daytime MODIS and AMSR-E have a larger bias in summer compared with winter, although in this case the negative
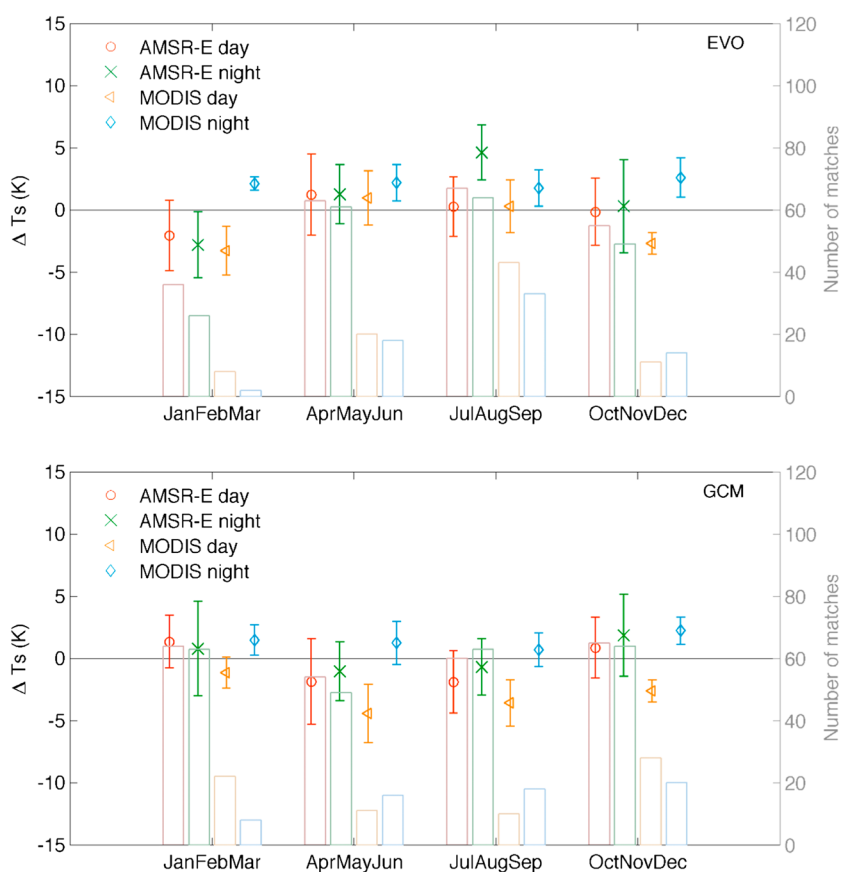
Figure 9. Seasonal statistics of the MODIS and AMSR-E T_s comparison with the in situ measurements at the (top) EVO and (bottom) GCM stations. The symbols (left y axis) give the satellite seasonal biases for nighttime/daytime as indicated in the legend, with the length of the line centered at each bias value showing the seasonal standard deviation of the difference. The number of matches (right y axis) is indicated by bars.

bias is in summer. The nighttime seasonal changes are less pronounced for AMSR-E, while MODIS bias is always positive for nighttime, similar to the EVO station. Figure 9 also illustrates again the much larger number of available AMSR-E T_s estimates, compared with MODIS (a ratio of ~3 for the EVO and GCM stations for most seasons).

It is difficult to identify the causes of this seasonal behavior, but we could hypothesize that something changes with season in either the representativeness of the station, or the quality of the T_s retrievals. Depending on land cover, the surroundings of the station might present some seasonal variability of surface conditions that is not represented at the station scale, resulting in seasonal discrepancies between the station and the satellite measurements. Regarding retrieval quality, snow conditions and occurrence and type of clouds are examples of seasonal changes that can have an impact for both microwave and infrared retrievals. Emissivity can also play a role: the MODIS retrieval uses a fixed emissivity, while the station T_s is processed with a seasonally changing emissivity, which can also induce changes in the comparison if the emissivity varies between seasons; for AMSR-E, the representativeness of the emissivity climatology can change along the year, with some seasons more prone to have large deviations from the expected surface conditions.

4.3. Evaluation Artifacts

Broken clouds can have an impact on the comparison between satellite and ground T_s estimates. This is illustrated in Figure 10, where time series of in situ, AMSR-E and MODIS T_s at the PSU station are plotted. To help the figure readability, the time series is plotted from 29 June to 4 July, but similar behavior was observed at other occasions at this station. The first 3 days are cloudy at daytime and MODIS T_s is not available. Scattered clouds are present and result in highly variable in situ T_s values due to the transition between shaded and nonshaded surfaces. At the AMSR-E scale this effect is attenuated given the spatial integration over a much larger area.
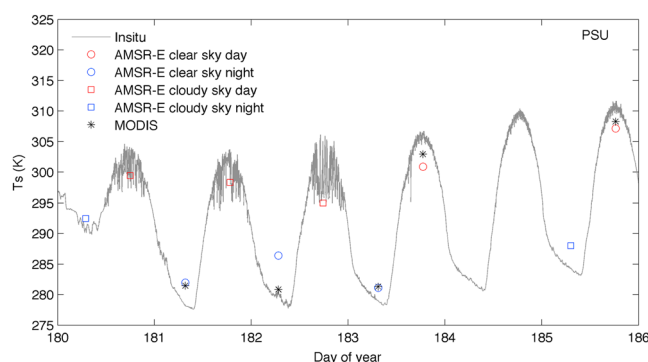
Figure 10. Example of in situ T_s time series at the PSU station. Plotted the 1 min sampled in situ T_s (solid line) from 29 June to 4 July 2010 and the available MODIS and AMSR-E estimates (symbols).

This in situ T_s variability linked to scattered clouds will penalize the AMSR-E cloudy-sky comparisons (compare with the clear-sky comparisons) for those stations and periods with frequent broken clouds.

Another source of instantaneous T_s variability impacting the comparisons is the changing location of the AMSR-E observations. The closest pixel to the station changes position at each satellite overpass. If surface heterogeneity at the station surroundings is significant, this will result in variability in the averaged MODIS and AMSR-E T_s that cannot be captured by the station measurements. Given the identified lack of surface homogeneity at the AMSR-E scale at most stations, it is very likely that this issue is contributing to the large STD observed at many stations. In principle, the impact of this will be larger for the AMSR-E observations. The largest dependence of microwave T_s in emissivity results in a larger T_s variability within the satellite footprint.

5. Summary

Inversions of AMSR-E brightness temperatures (T_{bs}) to derive land surface temperature (T_s) are presented. Targeting limited dependence on ancillary data sets and rapid conversion of T_{bs} into T_s estimates, the methodology is based on approximating the T_{bs}-T_s relationship by a global transfer function built by neural networks trained with a database of coincident AMSR-E T_{bs} and retrieved microwave T_s* from *Lipton et al.* [2015]. A close methodology was already presented in *Prigent et al.* [2016] to invert SSM/I observations, and similar to those inversions, climatological microwave emissivity (here from the database of *Moncet et al.* [2011]) is added as an input to the neural network together with the T_{bs} to help constraining the inversion problem.

The retrieval of T_s from microwave observations is subject to difficulties for some atmospheric surface conditions. They are mainly related to a rather large emissivity variability (e.g., related to snowpack metamorphism or changes in soil water content) and emission from subsurface layers for some specific soil types and conditions (e.g., sandy soils). To help identify these conditions, the inversion is accompanied by a coarse estimation of retrieval uncertainty based on estimating the retrieval error for a selection of T_s and emissivity conditions from the training database. Given that the target T_s* is already the product of an inversion, this retrieval uncertainty has to be consider as a low error estimate, with real uncertainty likely to be larger (i.e., the uncertainty with respect o the true T_s). For ~75% of the land surface the root-mean-square difference (RMSD, difference between the training target T_s* and the retrieved T_s by the neural network) is below 2.8 K.

To further characterize the inversions, a simple estimate of the quality of the retrieval and a series of flags to signal potentially difficult inversion situations are also provided. The estimate of retrieval quality is based on looking at the T_s variability from multiple trainings of the neural network with slightly different initial conditions. Regarding the flags, a series of ancillary products are used to identify snow and water covered ground, inversions close to the coastal line, atmospheric strong convection, and soils with large microwave penetration depth. For nonflagged inversions, where we expect the best retrieval performance, the retrieval variability shows median values of ~0.7 K. That value can reach close to 2.0 K for difficult inversions (e.g., over sandy soils with large microwave penetration depth).

Further strengths and issues of the T_s product are discussed by evaluating one year (2010) AMSR-E inversions at 10 selected ground stations. To provide a satellite infrared reference to the AMSR-E evaluations, MODIS T_s (MYD11A1, collection 5) [*Wan and Li*, 2008] is also compared to the station data. The MODIS T_s is averaged

over the 14×8 km resolution AMSR-E swath grid used for the T_s retrieval. Overall, MODIS agrees better with the station T_s than AMSR-E (all-station mean RMSD of 2.4 K for MODIS and 4.0 for AMSR-E), but MODIS being an infrared instrument, its measurements are limited to clear sky and are much more prone to contamination by undetected clouds. AMSR-E provides a much larger number of T_s estimates, with an approximated ratio of 3 to 1 over the analyzed stations. At many stations the RMSD of the AMSR-E clear sky and cloudy sky are comparable, highlighting the ability of the microwave inversions to provide T_s estimates under most atmospheric conditions. Closest level of agreement of MODIS and AMSR-E with the in situ T_s occurs at the temperate stations, likely the result of a more stable microwave emissivity well captured by the monthly climatological emissivity used for the inversions. Surface heterogeneity impacted the comparisons due to the large mismatch between the area-integrated satellite T_s and the point T_s estimate at the station. As the area surrounding the station is likely to be thermally more heterogeneous in the microwave than in the infrared, this may penalize the AMSR-E comparison. At a large number of stations the biases between the satellite and station T_s change sign between nighttime and daytime and were also noticed to seasonally change, but the causes of the observed patterns cannot be clearly identified. Further insight into the AMSR-E retrievals is given in Part 2, where a global comparison of the AMSR-E estimates with coincident satellite infrared T_s is presented.

Three years of AMSR-E T_s (2008–2010) have been produced so far and are archived at the GlobTemperature data portal (http://data.globtemperature.info) for public access. Further work will be targeting improvements on the processing of the original T_s^* to provide a more accurate T_b-T_s mapping, an extension of the time series to current years, and improvements on the uncertainty characterization. Given that a close methodology has been applied in *Prigent et al.* [2016] and here to invert T_{bs} from the family of SSM/I, SSMIS, AMSR-E, and AMSR2 sensors, work is planned for a common retrieval setup to offer a product with sampling at four distinct times of the day (close to midnight, early morning, midday, and late afternoon), allowing to characterize the diurnal cycle under most atmosphere surface conditions.

References

Aires, F., C. Prigent, W. Rossow, and M. Rothstein (2001), A new neural network approach including first-guess for retrieval of atmospheric water vapor, cloud liquid water path, surface temperature and emissivities over land from satellite microwave observations, *J. Geophys. Res.*, *106*, 14,887–14,907.

Aires, F., C. Prigent, F. Bernardo, C. Jimenez, R. Saunders, and P. Brunel (2011), A Tool to Estimate Land-Surface Emissivities at Microwave frequencies (TELSEM) for use in numerical weather prediction, *Q. J. R. Meteorol. Soc.*, *137*(656), 690–699.

Augustine, J. A., G. B. Hodges, and C. R. Cornwall (2005), An update on SURFRAD—The GCOS surface radiation budget network for the continental United States, *J. Atmos. Oceanic Technol.*, *22*(10), 1460–1472.

Aumann, H. H., et al. (2003), AIRS/AMSU/HSB on the aqua mission: Design, science objectives, data products, and processing systems, *IEEE Trans. Remote Sens.*, *41*, 253–264.

Ermida, S. L., I. F. Trigo, C. C. Dacamara, F.-M. Göttsche, F.-S. Olesen, and G. Hulley (2014), Validation of remotely sensed surface temperature over an oak woodland landscape—The problem of viewing and illumination geometries, *Remote Sens. Environ.*, *148*, 16–27.

Göttsche, F.-M., and G. C. Hulley (2012), Validation of six satellite-retrieved land surface emissivity products over two land cover types in a hyper-arid region, *Remote Sens. Environ.*, *124*, 149–158.

Göttsche, F.-M., F.-S. Olesen, I. Trigo, A. Bork-Unkelbach, and M. Martin (2016), Long term validation of land surface temperature retrieved from MSG/SEVIRI with continuous in-situ measurements in Africa, *Remote Sens.*, *8*, 410.

Hagan, M. T., and M. Menhaj (1994), Training feedforward networks with the Marquardt algorithm, *IEEE Trans. Neural Networks*, *5*, 989–993.

Koike, T. (2004), The coordinated enhanced observing period: An initial step for integrated global water cycle observation, *WMO Bull.*, *53*, 115–121.

Li, L., E. G. Njoku, E. Im, and P. Chang (2004), A preliminary survey of radio-frequency interference over the US in Aqua AMSR-E data, *IEEE Trans. Geosci. Remote Sens.*, *42*(2), 380–390.

Lipton, A. E., P. Liang, C. Jimenez, J.-L. Moncet, F. Aires, C. Prigent, R. Lynch, J. F. Galantowicz, R. P. d'Entremont, and G. Uymin (2015), Sources of discrepancies between satellite-derived and land surface model estimates of latent heat fluxes, *J. Geophys. Res. Atmos.*, *120*, 2325–2341, doi:10.1002/2014JD022641.

Martin, M., and F. Goöttsche (2015), Satellite LST validation report WP4-DEL-12, *Tech. Rep.*, ESA DUE GLOBTEMPERATURE Project, Karlsruhe Inst. of Technol., Karlsruhe, Germany. [Available at http://www.globtemperature.info.]

Moncet, J.-L., P. Liang, J. F. Galantowicz, A. E. Lipton, G. Uymin, C. Prigent, and C. Grassotti (2011), Land surface microwave emissivities derived from AMSR-E and MODIS measurements with advanced quality control, *J. Geophys. Res.*, *116*, D16104, doi:10.1029/2010JD015429.

Nguyen, D., and B. Widrow (1990), Improving the learning speed of 2-layer neural networks by choosing initial values of the adaptative weights. paper presented at 1990 International Joint Conference on Neural Networks (IJCNN), pp. 21–26, IEEE, New York, 17–21 Jun.

Prigent, C. (2005), Estimation of the aerodynamic roughness length in arid and semi-arid regions over the globe with the ERS scatterometer, *J. Geophys. Res.*, *110*, D09205, doi:10.1029/2004JD005370.

Prigent, C., E. Jaumouille, F. Chevallier, and F. Aires (2008), A Parameterization of the microwave land surface emissivity between 19 and 100 GHz, anchored to satellite-derived estimates, *IEEE Trans. Geosci. Remote Sens.*, *46*(2), 344–352.

Prigent, C., F. Papa, F. Aires, C. Jimenez, W. B. Rossow, and E. Matthews (2012), Changes in land surface water dynamics since the 1990s and relation to population pressure, *Geophys. Res. Lett.*, *39*, L08403, doi:10.1029/2012GL051276.

Prigent, C., C. Jimenez, and F. Aires (2016), Toward "all weather," long record, and real-time land surface temperature retrievals from microwave satellite observations, *J. Geophys. Res. Atmos.*, *121*, 5699–5717, doi:10.1002/2015JD024402.

Seemann, S. W., E. E. Borbas, R. O. Knuteson, G. R. Stephenson, and H.-L. Huang (2008), Development of a global infrared land surface emissivity database for application to clear sky sounding retrievals from multispectral satellite radiance measurements, *J. Appl. Meteorol. Climatol.*, *47*(1), 108–123.

Shcroft, P., and F. J. Wentz (2013), AMSR-E/Aqua L2A Global Swath Spatially-Resampled Brightness Temperatures, version 3, doi:10.5067/AMSR-E/AE_L2A.003.

Stokes, G. M., S. E. Schwartz, and J. R. Vacca (1994), The Atmospheric Radiation Measurement (ARM) program: Programmatic background and design of the cloud and radiation test bed, *Bull. Am. Meteorol. Soc.*, *75*(7), 1201–1221.

Takala, M., K. Luojus, J. Pulliainen, C. Derksen, J. Lemmetyinen, J.-P. Kärnä, J. Koskinen, and B. Bojkov (2011), Estimating northern hemisphere snow water equivalent for climate research through assimilation of space-borne radiometer data and ground-based measurements, *Remote Sens. Environ.*, *115*(12), 3517–3529.

Trigo, I. F., I. T. Monteiro, F. Olesen, and E. Kabsch (2008), An assessment of remotely sensed land surface temperature, *J. Geophys. Res.*, *113*, D17108, doi:10.1029/2008JD010035.

Trigo, I. F., et al. (2011), The satellite application facility for land surface analysis, *Int. J. Remote Sens.*, *32*(10), 2725–2744.

Wan, Z. (2008), New refinements and validation of the MODIS land-surface temperature/emissivity products, *Remote Sens. Environ.*, *112*(1), 59–74.

Wan, Z., and Z.-L. Li (2008), Radiance-based validation of the V5 MODIS land-surface temperature product, *Int. J. Remote Sens.*, *29*, 5373–5393.